Lyudmila Nyrkova, Larysa Goncharenko, Svetlana Osadchuk, Oleg Bratochkin*

E.O Paton Electric Welding Institute of the National Academy of Sciences of Ukraine, Kyiv, Ukraine

Scientific paper
ISSN 0351-9465, E-ISSN 2466-2585
https://doi.org/10.62638/ZasMat1337

Zastita Materijala 66 (4)
928 - 940 (2025)

Effect of thin-layer conditions on stress-corrosion cracking of x70 steel in near neutral pH soilution at cathodic polarisation

ABSTRACT

The priority task of modern underground main pipelines is to ensure the reliability of its operation, which largely depends on understanding the processes that occur on the surface of the pipes in the ground under conditions of cathodic protection. The purpose of this work is to study the features of stress-corrosion cracking (SCC) of X70 steel under conditions of thin-layer corrosion in near neutral pH environment. Potentiometry, voltammetry, massometry, electrolytic hydrogenation slow strain rate tests, scanning electronic microscopy were used. Differences in SCC mechanism of X70 steel at potentials of -0.950 V and -1.050 V in the investigated environments were experimentally determined. At -0.950 V, SCC of X70 steel in NS4 proceeds by anodic dissolution mechanism, and in the model soil environment - by mixed mechanism; at -1.050 V, SCC in the NS4 solution occurs by a mixed mechanism, and in a soil environment based on NS4 – by a hydrogen embrittlement mechanism. Obtained regularities are due to more significant embrittlement of the near-surface layer of the specimens in the model soil environment in thin layers under cathodic polarization, which leads to a change in SCC mechanism from plastic-brittle to completely brittle.

***Keywords**: pipe steel, slow strain rate tests, potentiometry, voltammetry, stress-corrosion cracking, thin-layer corrosion, hydrogenation*

1. INTRODUCTION

Corrosion of steel in soil is related to the influence of several factors, such as soil resistivity, concentration of dissolved salts and oxygen, moisture content, pH, concentration, and the presence of bacteria [1, 2]). One of the most influential factors in the corrosion of ferritic steels is soil moisture. Depending on the properties of the soil, local corrosion may occur at lower humidity levels.

Corrosion rate of steel increases with an increase in moisture content to a critical value showed that the corrosion rate of underground pipelines is inversely proportional to soil resistivity [3]. Dissolved oxygen in the soil forms areas of differential aeration, which accelerates steel corrosion. Suganya S. [4] emphasized that the rate and intensity of steel corrosion depend significantly on soil moisture and soil type. Therefore, corrosion in clay soil is more intense compared to corrosion in mixed and sandy soils.

Ezuber H.M. showed [5] that corrosion potentials have more negative values when soil moisture is increased. The rate of corrosion is maximum at humidity up to 20 % (by mass) for sand, and 25 % in clay, saline, and limestone soils. Corrosion activity of soil at critical soil moisture increases in the order:

calcareous < clay < saline < sand.

Zhang L. [6] found that temperature, dissolved oxygen concentration, and pH have a significant effect on the corrosion current density (i_{corr}) of X70 steel: the corrosion of X70 steel is the least in a weakly acidic environment with low temperature and oxygen deficiency.

Attention is drawn to the work of Jiang J. [7], who introduced the role of a three-phase boundary (gas/liquid/solid) on the pipeline surface. He states that the distribution of the liquid on the metal surface depending on the length of the gas/liquid/solid three-phase boundary is an important property of the medium, it was found that both the limiting diffusion current and the corrosion current density increase linearly with the length of the three-phase boundary, indicating that the cathodic and corrosion processes in such systems depend not only on the thickness of the liquid layer but also strongly on the state of distribution of the liquid on the metal surface.

*Corresponding author: Lyudmila Nyrkova
E-mail:lnyrkova@gmail.com
Paper received: 11.01.2025.
Paper accepted: 23.01.2025.

Liu H. [8] demonstrated that the maximum corrosion rate is determined in a 5 mm thick soil layer due to the competing effects of the blocking effect of the soil layer and its ability to retain moisture for corrosion to occur. In thin soil layers, corrosion accelerates with increasing soil thickness due to the greater amount of water contained in it. When the thickness of the soil layer increases to more than 5 mm, the soil begins to block the diffusion of ions involved in the corrosion process. Steel corrosion also strongly depends on the permeability of gases in the soil: the rate of steel corrosion is highest in aerobic soil, and the maximum rate of local steel corrosion is determined in a 3 mm thick soil layer with free air access is 0.72 mm/year, the rate of uniform corrosion is 0.04 mm/year.

Research by Wang S. [9] showed a decrease in the corrosion rate of X70 steel in red soil with time, according to an exponential law. The corrosion was uniform with uneven and localized pitting, and α-FeOOH was the dominant corrosion product with good protective properties.

Song Y. [10] showed that chlorine ions affect the properties of corrosion products due to their participation in reactions. Along with α-FeOOH, γ-FeOOH, and iron oxides, at high chloride concentrations, β-Fe8O8(OH)8Cl1.35 was more likely to form than β-FeOOH.

And Bai X. [11] reported on the strong adsorption capacity of chloride ions on X80 steel at temperatures above the freezing point. At temperatures below the freezing point, sulfate ions present in the pore solution of the soil contribute to its swelling and deformation, which makes X80 steel more prone to corrosion in sulfate-containing environments.

Pipe steels X70, X80, X100, and X120 in acidic soil, alkaline soil, and dry sandy soil in China are prone to stress-corrosion cracking when tested on U-shaped and slotted specimens [12]. Susceptibility to SCC increased with increasing steel strength and decreasing soil pH. In acidic soil, there was no relationship between the locations of SCC cracks and the occurrence of pitting. In alkaline soil, SCC cracks mainly occurred at the bottom of the pittings.

Fu A.Q. [13] showed that in thin layer of 60 μm of near neutral pH solution, steel can be passivated due to the saturation of a thin layer of an aqueous solution of Fe^{2+}. As the thickness of the solution layer increases, its saturation by Fe^{2+} is more difficult to achieve, so passivity is not maintained, and the steel undergoes active dissolution. The rate of anodic dissolution of steel increases with immersion time. In the thin layer of the solution, diffusion and reduction of oxygen dominate in the cathodic process, which is evidenced by the presence of a limiting diffusion current. In the volume of the solution, the absence of the limiting diffusion current on the cathodic polarization curve indicates that the main cathodic reaction is the reduction of H_2CO_3 and HCO_3^-, and thus the composition of the formed film is dominated by $FeCO_3$.

Yan M. [14] states that there is an environment with an almost neutral pH beneath the disbonded coating. The effectiveness of cathodic protection and the protective effect under the exfoliated coating can be evaluated by measuring pH of the thin electrolyte layer under the disbonded coating.

When wetting/drying cycles change, stress-corrosion cracking mechanism of X100 steel at low pH and high dry/wet ratio includes anodic dissolution and hydrogen reduction [15].

In a simulated acidic soil solution, X70 steel is susceptible to stress-corrosion cracking under cathodic polarization, which manifests itself in loss of viscosity and brittle failure. The lower the polarization current, the faster stress-corrosion cracking occurs. Stress has a synergistic effect with electrochemical reactions to accelerate the cathodic evolution of hydrogen, making X70 steel more susceptible to stress-corrosion cracking [16].

Studies of the change in moisture content (20-100 wt. %) on the electrochemical behavior of X70 pipe steel in Skikda soil showed that the corrosion current is directly proportional to the moisture content up to a moisture content of 50 wt. % [17]. It was revealed pitting corrosion of X70 steel at the soil moisture content of 20 % by mass., and the further development of pitting corrosion at a humidity of 50 % by mass. However, when the moisture content exceeded 50 %, the surface became completely covered with corrosion products. X-ray structural analysis revealed the dominance of FeOOH and Fe_3O_4 phases on the steel surface at a moisture content of 50 % by mass.

Analyzing the results presented in the literature, we came across the fact that researchers have focused on the study of corrosion and electrochemical processes occurring in steel, but one of the most dangerous phenomena – stress-corrosion cracking of underground gas pipelines – taking into account the influence of thin-film corrosion–remains completely unexplained. Underground gas pipelines are operated under complex anti-corrosion protection: passive (protective polymer coatings) and active (by introducing cathodic polarization). As experience shows, even when operating conditions are observed following current regulatory documents, the phenomenon of stress-corrosion cracking

develops over time. This work is devoted to the study of steel corrosion in soil under the joint influence of stress and cathodic polarization. In thin films of soil electrolyte formed on the surface of steel in a defect of the protective coating in the soil with limited access of oxygen, corrosion processes are accelerated, and the regularities of stress-corrosion cracking may differ from those in the solution. Therefore, the purpose of this study is to investigate the regularities of the phenomenon of stress-corrosion cracking of pipe steel X70 in a model soil with almost neutral pH under cathodic polarization, and to establish possible differences in the development of this phenomenon compared to the regularities in a model soil electrolyte. The novelty and originality of this study lies in the application of new methodological approaches to the study of the specified phenomenon, with the help of which new data will be obtained on the regularities of stress-corrosion cracking of pipe steel in soil conditions. These results will be a significant contribution to understanding the phenomenon of stress-corrosion cracking and will be of practical interest to organizations operating underground gas pipelines.

2. EXPERIMENTAL

Investigations was carried out on X70 steel specimens with a ferrite-pearlite structure made from sheets of controllable rolling, Fig. 1.

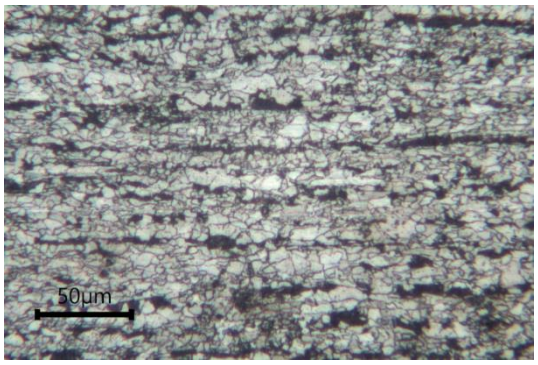

Figure 1. Microstructure of X70 steel

The chemical composition of the metal was determined by the spectral method using the Spektrovak-1000 device manufactured by the Biardcompany and presented in **Table 1**.

Table 1. Chemical composition of steel

Mn	C	Si	P	S	Nb	Mo	V	Ti	Ni	B
1.71	0.10	0.21	0.01	0.01	0.05	0.03	0.06	0.02	0.03	0.002

Mechanical properties of steel: yield strength not less than 485 MPa, strength limit not less than 570 MPa, relative elongation not more than 20 % [18].

Specimens were cut from a steel sheet across the rolling according to the sketch in Fig. 2.

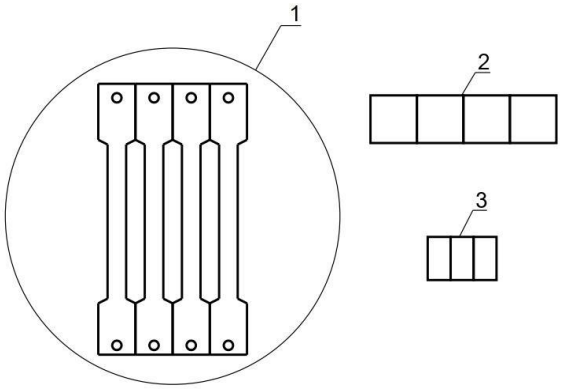

Figure 2. Specimens cutting scheme for various types of research: 1 – corrosion-mechanical tests; 2 – electrolytic hydrogenation tests; 3 – corrosion rate determination

The research solution is a model soil electrolyte NS4, g/l: 0.122 KCl + 0.483 $NaHCO_3$ + 0.181 $CaCl_2$ + 0.131 $MgSO_4$ [19]. For the preparation of the solution, distilled water and pure analytical reagents were used. The reagents were weighed on analytical laboratory scales VLR-200g.

The surface of the specimens was cleaned with sandpaper of different grain sizes, degreased with magnesium oxide, washed with running water, then with distilled water, and dried with filter paper. For electrochemical measurement pressure cell was used.

Potentials were measured against saturated KCl silver chloride reference electrode (SSCE) for 1 hour using MTechPGP-550Fpotentiostat. In all measurements (cathodic and anodic polarization curves, fast and slow polarization curves, slow strain rate tests) the standard three-electrode system was used: steel as a research electrode, the saturated KCl silver-chloride electrode as the reference electrode, and the Pt wire as the auxiliary electrode. For cathodic and anodic polarization curves potentiodynamic mode and potential sweep rate of 1 mV/s was used. Polarization curves of fast and slow potential scan rate, 0.5 mV/s and 100 mV/s, relatively, were measured from -1,200 V to 0.500 V. All results are averaged over three measurements.

Sketch of a specimen for corrosion-mechanical slow strain rate tests show in **Fig. 3**. Corrosion-mechanical studies were carried out with slow strain rate tests (10^{-6} s^{-1}) on the AIMA-5-1 breaking machine with periodic wetting with the solution for 50 min in the solution, 10 min in air, and in sand moistened with NS4 solution to 20 % humidity. The slow strain rate tests were carried out at cathodic polarization -0.950 V, -1.050, and -1.200 V (relative

to SSCE) using a PI-50-1.1 potentiostat.potentials of -0.750 V,

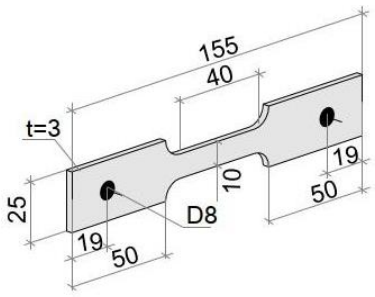

Figure 3. Sketch of a specimen for corrosion-mechanical slow strain rate tests

The study of hydrogen permeation into X70 steel was carried out according to the methodology described in detail in our previous works [20, 21]. The research was carried out at cathodic polarization potentials of -0.750 V, -0.950 V, -1.050 V, and -1.200 V. The concentration of hydrogen penetrating the steel specimen was calculated by the formula:

$$C_0 = \frac{kL}{D_{H_2} FS} \quad C_0 = \frac{I_{st} \cdot L}{D_{H_2} \cdot F \cdot S} \qquad (1)$$

I_{st} – current strength in the stationary regime of hydrogen penetration, A;

S – specimen square, m^2(0,00096 m^2);

F – Faraday constant (96485 C/mol);

D_{ef} – coefficient of effective diffusion of hydrogen in steel ($1.5 \cdot 10^{-9}$ cm^2/s);

C_0 – concentration of hydrogen penetrating through steel, mol/m^3;

L – specimen thickness, m.

The coefficient of effective diffusion of hydrogen in steel, based on the time for fulfillment the condition $J(t)/J_{st}$=0.63, was calculated by the formula:

$$D_{ef} = \frac{L^2}{6t_{0.63}} \qquad (2)$$

where $t_{0.63}$ - time to reach the value $J(t)/J_{st}$=0,63.

J_{st} – hydrogen penetration flow through the steel on the oxidizing side of the specimen at a steady state, mol/(m^2·s);

$$I_{st} = I_{H2} - I_B \qquad (3)$$

I_{H2} – current strength due to hydrogen penetration, A;

I_B – background current corresponding to the passivation current of the specimen, A.

The corrosion rate was determined by massometry based on the change in specimen mass and research duration.

Specimens for metallographic studies were made according to the standard method using diamond pastes of different dispersions. To reveal the microstructure, the specimens were etched in a solution of 4 % nitric acid in ethyl alcohol. Metallographic studies were performed on a NEOPHOT 21 microscope using an Allied Vision 1800 U-2050c digital camera and SEOImageLAB software.

The fracture surface after slow strain rate tests was examined by scanning electron microscopy on JSM 840 microscope (JEOL, Japan) in the mode of secondary backscattered electrons at an accelerating voltage of 20 kV and an electron beam current of (10^{-7}-$10 \cdot 10^{-10}$) A.

3. EXPERIMENTAL RESULTS

3.1. Determination of the corrosion rate

After testing the specimens in the NS4 solution, corrosion products are dark, almost black color were formed (Fig. 4). After exposure of the specimens in a model soil environment based on NS4, the surface is covered with an uneven layer of corrosion products with grains of sand firmly attached to the surface, black and brown corrosion products. Corrosion rate values in NS4 solution and NS4-based soil environment are very close, 0.0536 mm/year and 0.0563 mm/year.

Figure 4. Appearance of specimens after tests for 168 hours at room temperature in environments: 1 – NS4; 2 – model soil environment based on NS4

3.2. Electrochemical investigations

Corrosion potential of X70 steel in the NS4 solution was -0.737 mV, in the soil environment corrosion potentials is positively by 33 mV, -0.704 V (**Fig. 5**). The anodic slopes are equal to 0.063 V and 0.059 V, correspondingly (**Table 2**). This indicates that the mechanism of anodic dissolution in the conditions of thin layer corrosion controlled by diffusion of oxygen. But in the model soil environment, some difficulty in the anodic reaction was noted due to slowing of oxygen access to the surface. The electrochemical data are satisfactorily

correlated with the results of the corrosion rate determining, which is equal to 0.0536 mm/year in the NS4 solution and 0.0563 mm/year in the soil environment.

It was established that null current potentials for X70 steel in the NS4 solution are, respectively: -1.001 V and -1.085 (Fig. 6, a). Therefore, in the NS4 solution, in the range of potentials more positive than -1.001 V, stress-corrosion cracking proceeds by the anodic dissolution mechanism, at potentials negatively -1.085 V – by hydrogen embrittlement mechanism. In the range of potentials from -1.001 V to -1.085 V, stress-corrosion cracking proceeds by a mixed mechanism – anodic dissolution and hydrogen embrittlement.

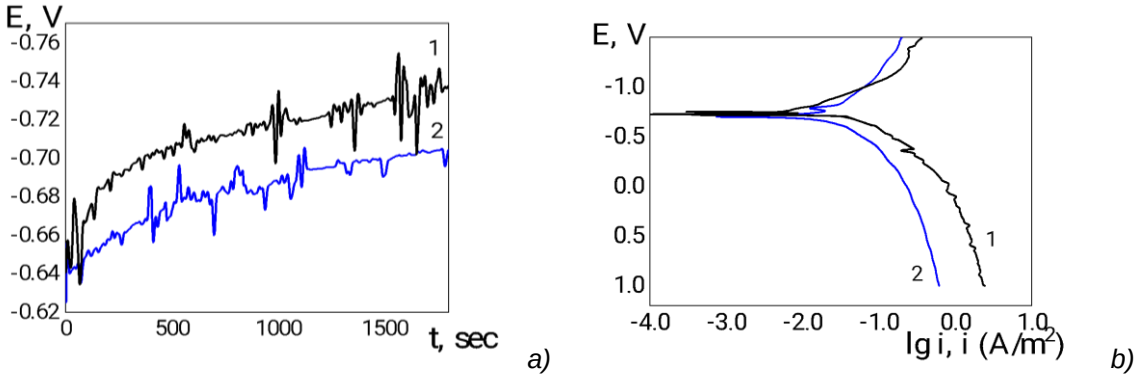

Figure 5. Corrosion potentials (a) and polarization curves (b) of X70 steel: 1 – NS4 solution; 2 – model soil environment based on NS4

Table 2. Electrochemical and corrosion properties of X70 steel in near neutral pH environments

Environment	E_{cor}, V	b_a, V	$E^1_{i=0}$, V	$E^2_{i=0}$	v_{cor}, mm/year
NS4	-0.737	0.063	-1.001	-1.085	0.0536
Soil environment on the base of NS4	-0.704	0.059	-0.926	-1.050	0.0563

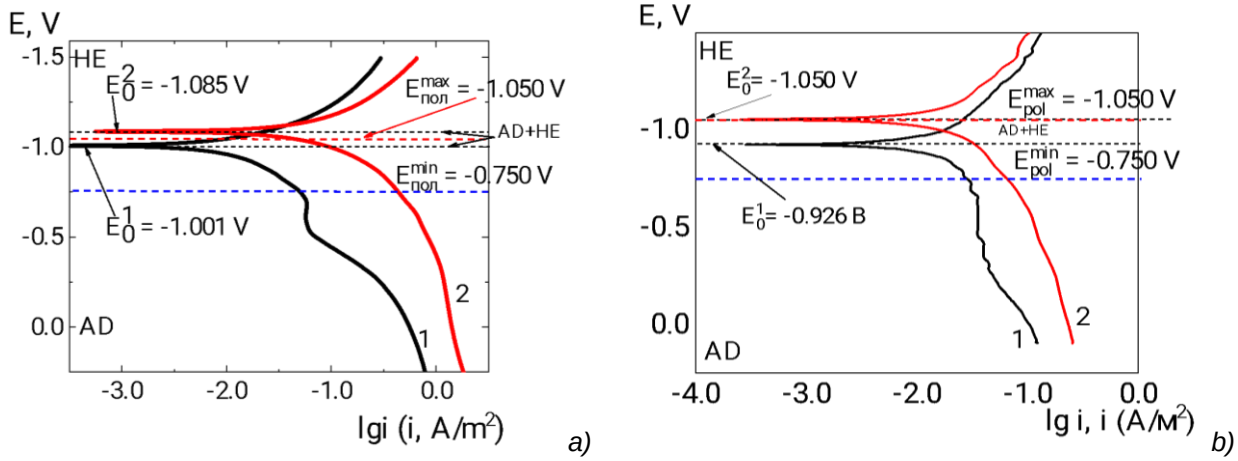

Figure 6.Potentiodynamic polarization curves of X70 steel in a NS4 solution (a) and in a model soil environment based on NS4 (b), at a potential scanning rate: 1 – 0.5 mV/s; 2 – 100 mV/s

In the model environment, the null current potentials are, respectively: -0.926 V and -1.050 (Fig. 6, b). Therefore, in the model medium in the range of potentials more positive than -0.926 V, stress-corrosion cracking proceeds by the mechanism of anodic dissolution, at potentials more negative than -1.050 V – by the mechanism of hydrogen embrittlement. In the range of potentials from -0.926 V to -1.050 V, stress-corrosion cracking proceeds according to a mixed mechanism – anodic dissolution and hydrogen embrittlement. Some expansion of the range of the mixed mechanism for the NS4-based soil environment can be noted.

3.3. Slow strain rate tests

Breaking diagrams of specimens in the model soil electrolyte NS4 and the model soil environment based on NS4 are shown in Fig. 7.

Destruction in air is accompanied by narrowing the specimens near the place of rupture, as a result of which areas that have undergone plastic deformation are formed, Fig. 8, a. The breaking time was 44 hours, the relative elongation was 28.5 %, the susceptibility to SCC coefficient K_s was 1.03 (Table 3).

The coefficient of susceptibility to stress-corrosion cracking $_{KS}$ was calculated according to the formula [22, 23]:

$$K_S = \left(\frac{S_0 - S_1^{air}}{S_0}\right) \Big/ \left(\frac{S_0 - S_1^{env}}{S_0}\right) = \frac{\Psi_{air}}{\Psi_{env}} \quad (4)$$

Where Ψ_{air} and Ψ_{env} are the relative reduction in area of specimens, respectively, in air and in the corrosive environment;

S_0 is the cross-section area of specimens before tests, mm²;

S_1^{air} is the cross-section area of specimens in the in the fracture site after tests in air, mm²;

S_1^{env} is the cross-section area of specimens in the fracture site after tests in the corrosive environment, mm².

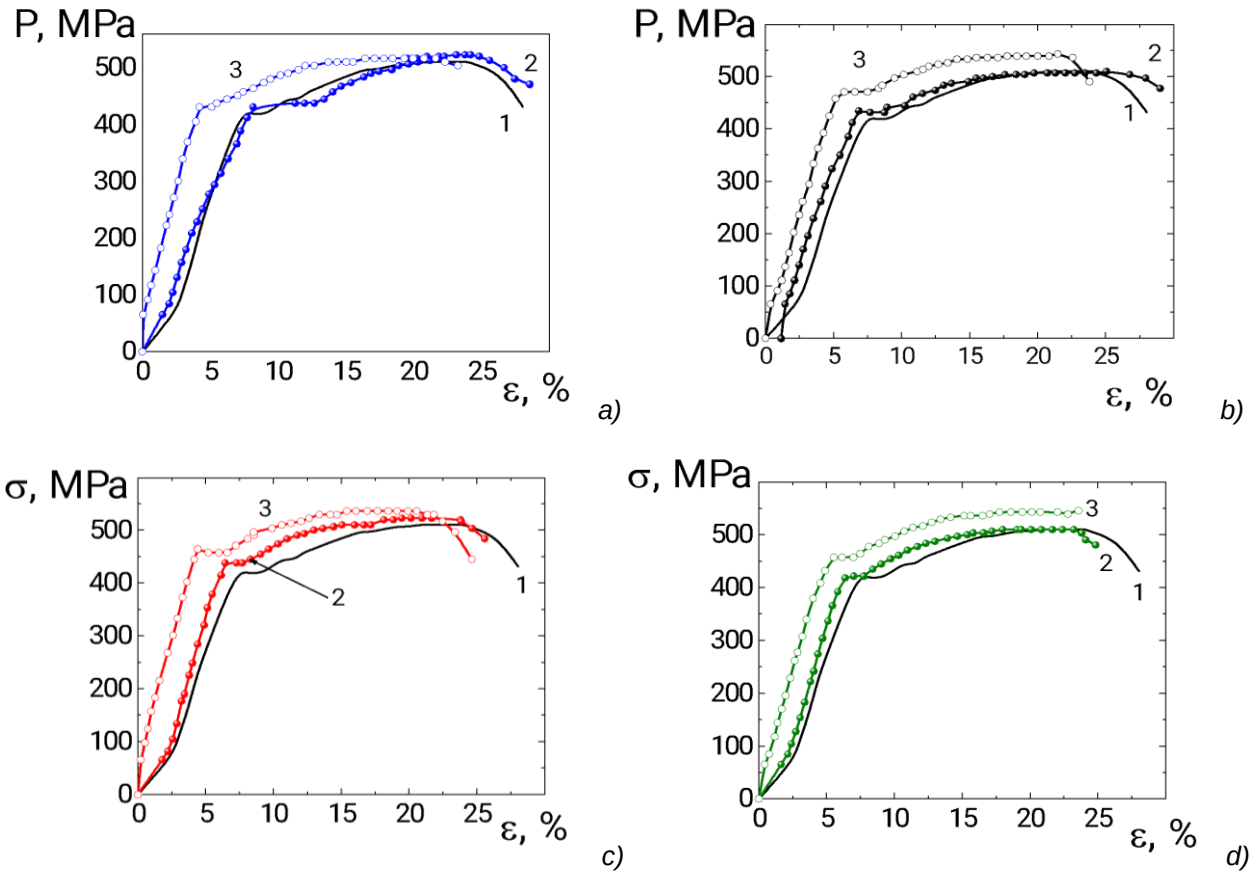

Figure 7. Breaking curves of X70 steel specimens after slow strain rate tests in air (1), in model soil electrolyte NS4 (2) and model soil environment based on NS4(3) at polarization potentials: a – -0.750 V ; b – -0.950 V; c – -1.050 V; d – 1.200 V

At a polarization potential from the region of anodic dissolution of -0.750 V, i.e., the minimum protective potential according to DSTU 4219 [24] in the NS4 solution, the destruction also occurred mainly viscously, the rupture line is wavy, but more complex than in air (Figure 8, b). The time of destruction was 44 hours, the relative elongation was 28.5 %, the relative contraction decreased to 72.57 % (Table 3). The coefficient of susceptibility to stress-corrosion cracking K_s is 1.03.

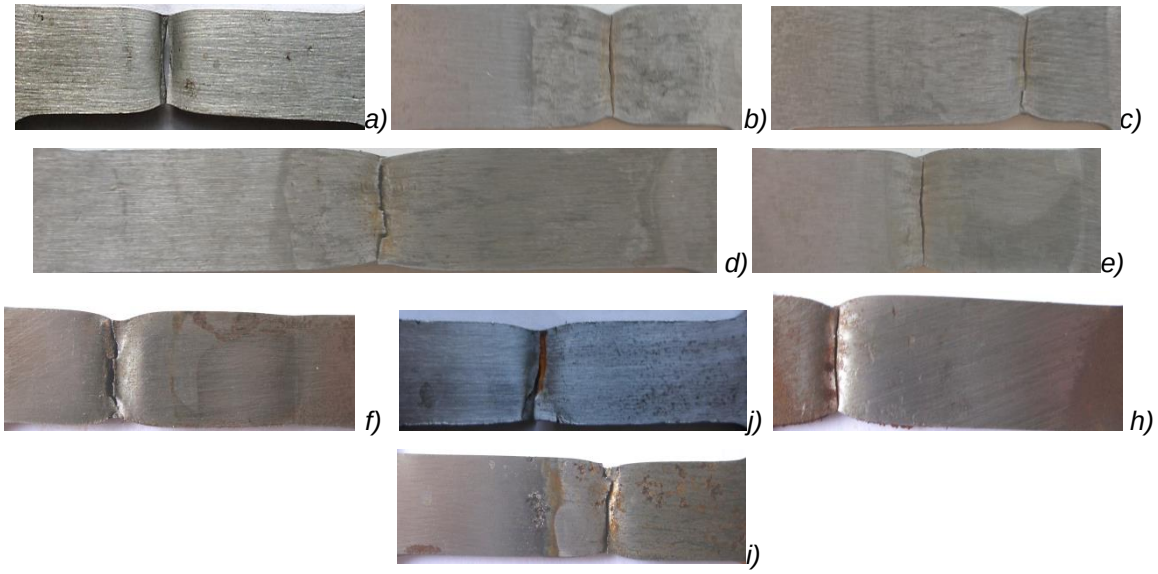

Figure 8.The rupture area of X70 steel specimens after slow strain rate tests in air (a), in a model soil electrolyte NS4 (b-e) and in a model soil environment based on NS4 (f-i) at polarization potentials: b, f – -0.750 V; c, j – -0.950 V; d, h – -1.050 V; e, i – 1.200 V

Table 3.Mechanical properties of X70 steel in air and corrosion-mechanical properties in NS4 model soil electrolyte and in NS4-based soil medium at different polarization potentials

Test conditions, potential, V	τ_{break}, h	δ_{TM}, %	S, mm²	Ψ, %	K_S	Breaking surface characterization
Air	43	28.00	7,51	74,95	-	Viscous
NS4						
-0.750	44	28.5	8.23	72.57	1.03	Mostly viscous
-0.950	41	29.0	9.36	68.80	1.09	Mostly viscous
-1.050	39	25.6	10.40	65.31	1.15	Viscous with brittle fragments
- 1.200	39	24.8	13.91	53.6	1.40	Mostly brittle
Modes soil environment based on NS4						
-0.750 B	39	23.2	7.21	75.94	1.00	Mostly viscous
-0.950	39	23.81	11.28	62.41	1.20	Viscous with brittle fragments
-1.050	41	24.6	11.83	60.55	1.24	Viscous with brittle fragments
-1.200	41	23.6	15.41	48.64	1.54	Mostly brittle

Tests at a polarization potential of -0.950 V in the NS4 electrolyte showed that the destruction of the specimen on a larger surface area is viscous (Fig. 8, c). At this potential, a decrease in the time of destruction of the samples was observed to 41 hours, and a relative narrowing to 68.80 %, but the relative elongation slightly increased to 29.0 % (Table 3). The K_s coefficient increased to 1.09 (Table 3).

At the maximum protective potential of -1.050 V, the brittle character prevails in the destruction, the narrowing of the specimens is noticeably less, Table 3, the rupture line is a stepped-like fracture with visible secondary cracks (Fig. 8, d). The destruction time of the specimens continued to decrease to 39 hours, the relative elongation to25.6 %, the relative narrowing to 65.31 % (Table 3). The value of the coefficient of susceptibility to stress-corrosion cracking has increased to 1.15.

At a potential greater than the value of maximum protective, -1.200 V, a decrease in relative elongation to 24.8 %, relative narrowing to 53.6 %, and an increase in K_s to 1.40 were noted (Table 3). The fracture line is complexly polyline (Fig. 8, e).

In a model soil environment based on NS4 at a minimum protective potential of -0.750 V, the failure also occurred mainly viscously and is accompanied by visually noticeable plastic deformation of the sample (Fig. 8, f), but the time of failure and relative elongation is less than for the specimens in solution – 39 hours and 23.2 %. In

contrast to the patterns of rupture in the solution, the relative narrowing was greater, 75.94 % (Table 3), and the coefficient of susceptibility to stress-corrosion cracking K_s was equal to 1.00.

After the destruction of the specimens in the model soil environment based on NS4 at a potential of -0.950 V, the rupture line is broken, secondary cracks are visible on the surface (Fig. 8, j). The specimen destruction time was 39 hours, a slight increase in relative elongation to 23.81 % and a decrease in relative narrowing to 62.55 % were observed (Table3). The K_s coefficient increased to 1.20 (Table 3).

At the maximum protective potential of -1.050 V, plastic deformation of the specimen is also noted (Fig. 8, h). The destruction time of the specimens was 41 hours, and the relative elongation increased to 24.6 %, the relative narrowing decreased to 60.55 % (Table 3), which contributed to the growth of the coefficient of susceptibility to stress-corrosion cracking K_s to 1.24.

At a potential greater than the maximum protective value, -1.200 V, a decrease in the relative elongation of the specimen to 23.6 % was noted, compared to the relative elongation in solutions under the same conditions, and a rather significant decrease in the relative narrowing to 48.64 %, and an increase in K_s to 1.54. The fracture line is complex fracture, secondary cracks are revealed (Fig. 8, i).

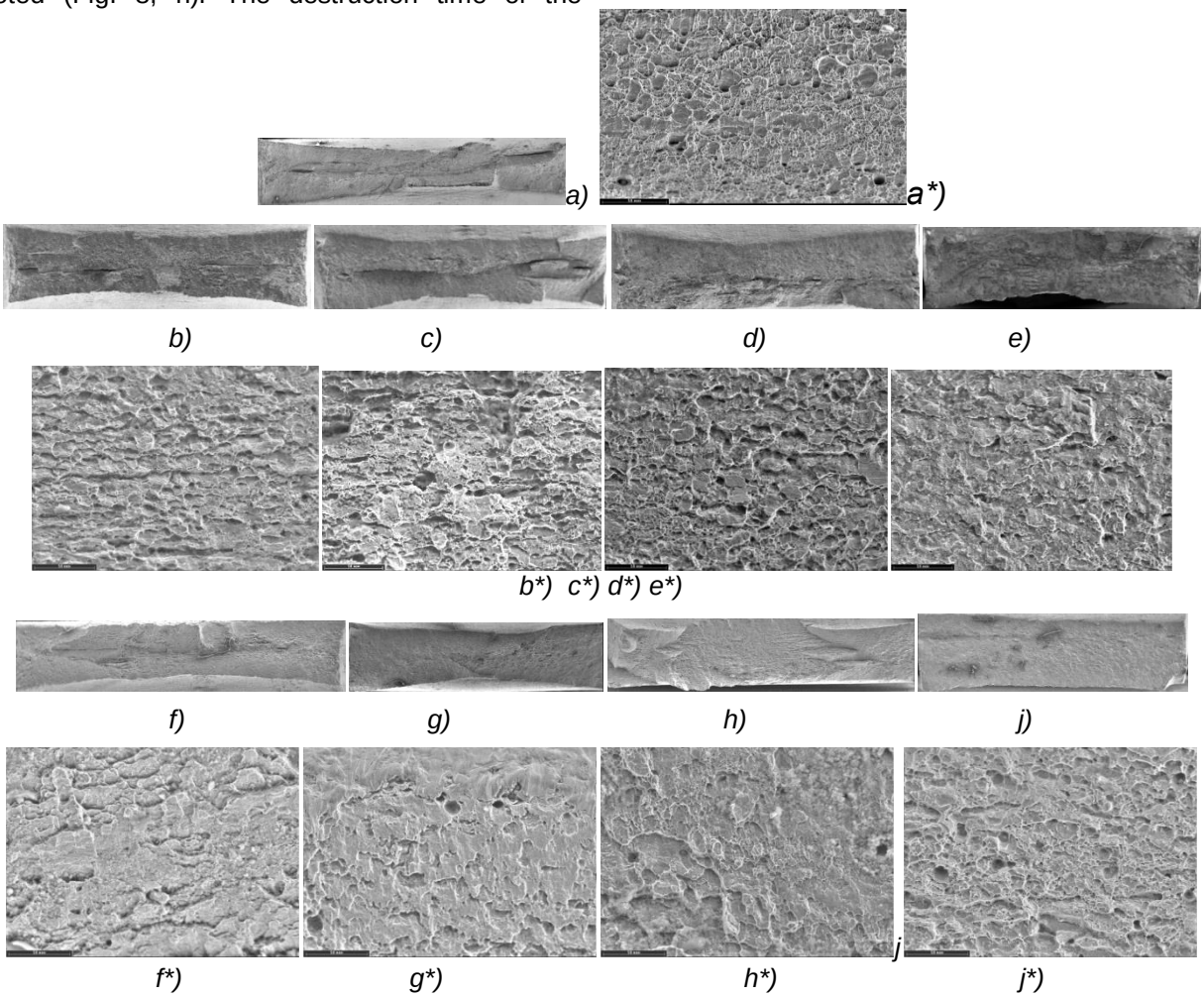

Figure 9. Fracture surfaces of X70 steel specimens after mechanical tests in air (a, a), corrosion-mechanical tests in a model soil electrolyte NS4 (b-e, b*-e*) and in a model soil environment based on NS4 (f-i, f*-i*) at polarization potentials: b, b*, f, f* -0.750 V; c, c*, g, g* – -0.950 V; d, d*, h, h* – -1.050 V; e, e*, i, i* – -1.200 V*

3.4. Fracture graphic investigations

The fracture surface of the specimen after rupture in air is complex, completely fibrous, and without brittle fracture with pronounced signs of plastic deformation (Fig. 9, a), which are especially noticeable in deep dimples formed due to small

non-metallic inclusions. Along with the main zones of viscous dimple failure by detachment, elements of viscous shear failure are observed. The size of pits during rupture corresponds to the size of grains, subgrains, which are visible on metallographic sections, as well as the distance between inclusions. The fractographic picture of the fracture surface is complicated by the striation of the distribution of structural elements in the form of pearlite bands, which are formed in steel produced using controllable rolling. Larger flat dimples are the result of shear destruction of pearlite colonies (grain size approximately 22 μm) under the action of intense plastic deformation. Pearlite streaks are the result of controllable rolling during steelmaking.

The fractographic details of the topography after the rupture of the specimens in the solution NS4 at a potential of -0.750 V indicate the viscous dimple nature of the fracture. Larger dimples indicate on the destruction by shear and detachment (Fig. 9, b, b*). In addition, the dimples are elongated in the direction of the rolling of the steel, which is associated with the elongated structure of its grains. In some zones of pore fusion, shear facets are observed, which were formed by the fusion of pores and the deformation. The fractogram also revealed the area of the initial stage of the formation of cleavage. In general, fracture fragments differ a little from the fracture of a specimen ruptured in the air.

The appearance of the breaking fracture at a potential of -0.95 V differs by greater heterogeneity – a variety from the topography of the fracture that occurred in air (Fig. 9, c, c*). Along with the plastic shear when the specimen ruptured, the destruction was accompanied by the formation of dimples of different diameters. For the most part of area, these dimples are small and shallow, with a lower energy density compared to air, and there are also deep pits, as can be seen, with non-metallic inclusions at the bottom. Also, many flat zones are visible on the fracture – chipping facets, after the separation of the united small pores, with poorly developed viscous bridges, as well as when the pearlite grains, present in the form of strips of rolled steel, are separated. At the fracture, there are small splits, which are characteristic of controllable rolling steel during plastic deformation. The appearance of quasi-crack facets with a size of up to 20 μm is noted. It should also be noted separately that there are several local loose zones without plastic deformation signs, which can be assumed to be the result of hydrogen damage to the metal.

At the maximum protective potential of -1.050 V, a change in the state of the metal was detected on the fracture surface in local zones, presumably in the zones of hydrogen penetration due to tensile stresses and cathodic polarization (Fig. 9, d, d*). The nature of the fracture of the specimens is mixed: along with small pits that occupy an insignificant part of the surface, elements of brittle fracture were found – chip facets of intergranular fracture (with a maximum diameter of approximately 30 μm), deep pits (with a diameter of approximately 20 μm) and smaller dimples from intergranular fractures at the bottom of which the carbide phase is manifested. The proportion of dimple viscous failure is much smaller compared to brittle failure.

A small part of the fracture surface of specimen at a potential of -1.200 V in the NS4 solution (closer to the specimen edge) contains fragile chipped facets (Fig. 9, e, e*). Pits of different sizes are observed, formed by the union of smaller pits, including at the plane of viscous shear, which indicates the presence of plastic deformation. Thus, the type of failure under these conditions can be attributed to a mixed viscous-brittle nature. The nature of the destruction is significantly different from that which was observed at the minimum protective potential of -0.750 V.

Destruction at a potential of -0.750 V in a model soil medium based on NS4 corresponds to a fully viscous nature (Fig. 9, f, f*). It can be distinguished that the structure of the components of the fracture surface was formed due to the unification of small pores into fragments and shear deformation in the plastic region.

After rupture at a potential of -0.950 V, the topography of the surface changed: most of it corresponds to a viscous nature due to plastic destruction as a result of shear deformation (Fig. 9, g, g*); the other part consists of fragments in the form of shallow and mostly large flat pits up to 25 μm in size, destroyed by detachment, which were formed by the union of a large number of pores. In addition, there are already quasi-crack facets up to 20 μm in size in the fracture. Several round, larger, and deeper pits compared to the fracture in the air fracture were also found, possibly from the additional impact of hydrogen penetration and the test environment.

As evidenced by the analysis of the fracture surface at -1.050 V, a change in the state of the metal was noted in individual local zones with a diameter of approximately 110 μm(Fig. 9, h, h*), which are larger than those formed on the fracture surface of the specimen during tests in the NS4 solution. It is assumed that this is a consequence of the selective penetration of hydrogen into the metal. In the specified zones, the mechanism of mixed destruction was realized, which manifests

itself in elements of low-energy intergranular microcracks with the merging of micropores. The facets of the quasi-cleavage are connected by separation ridges and shallow pits. Such a mechanism can be manifested in low-alloy steels in the temperature range of the brittle-viscous transition. Partially, closer to the surface of the sample, the mechanism of intergranular fracture is implemented. As can be seen, the facets of the chip are not very distinct, they are shallow pits connected by ridges of detachment. At the bottom of the facets, a slat structure can be traced.

The fractographic components of the fracture surface of the specimens at a potential of -1.200 V indicate a developed, mainly pitted character (Fig. 9, i, i*). Attention should be paid to the presence of large dimples, including those with small inclusions visible at the bottom, and pits of different sizes formed by shear due to the merging of smaller pores. Small defects could serve as traps for hydrogen, which was actively released at such a polarization potential, with their subsequent growth and transformation into larger, deep, round and elongated pits.

4. DISCUSSION

Under free corrosion conditions, the corrosion rates of steel X70 in both environments have similar values, but in the model soil environment, the corrosion rate is 5 % higher. The mechanism of anodic dissolution does not change, which is confirmed by the slopes of the anodic curves. Corrosion potentials in the solution are negatively than in the model soil environment, which correlates with the data of other authors (Ezuber H.M. et al. 2021).

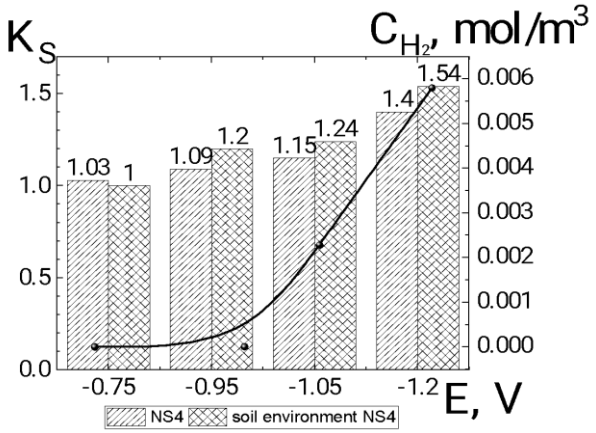

Figure 10.Susceptibility to hydrogenation of X70 steel (line) and susceptibility to stress-corrosion cracking (columns) of specimens after slow strain rate tests in a model soil electrolyte NS4 and a model soil environment based on NS4 depending on the cathodic polarization potentials

At cathodic polarization potentials from -0.750 V to -1.200 V in the model soil environment based on NS4, the relative elongation is significantly less than in the NS4 solution (Fig. 7), which indicates an increased tendency to brittle failure in this environment (Table 3). The susceptibility to stress-corrosion cracking of X70 steel increases most intensively when the potential shifts from -0.950 V to -1.200 for both environments, which is due to an increase in hydrogen permeating through steel (Fig. 10), and in the NS4 model soil electrolyte, the susceptibility to stress-corrosion cracking is higher than in NS4 solution.

At a minimum protective potential of -0.750 V, the susceptibility to stress-corrosion cracking of X70 steel in both environments is almost the same, the K_s coefficient is equal to 1.03 for the NS4 solution and 1.0 for the model soil environment, respectively. Breaking in the NS4 solution occurred mainly by the detachment of small pores, including when they were joined, with a small contribution of the shear force component. In the soil environment, the fracture of the specimen is also ductile, but due to the shear force in the plastic region. There were no noticeable changes in the fracture surface compared to the fracture surface of the specimens in air, both for the solution and for the soil environment.

The greatest differences in susceptibility to stress-corrosion cracking occurred at potentials of -0.950 V and -1.050 V, in particular, differences in the mechanism of stress-corrosion cracking were established. Therefore, at a potential of -0.950 V (between the minimum and maximum protective potential), stress-corrosion cracking of X70 steel in the NS4 solution proceeds by the anodic dissolution mechanism, and in the model soil environment based on NS4 – by the mixed mechanism. The coefficient of susceptibility to stress-corrosion cracking K_s in the model soil environment is greater than that of the NS4 solution, 1.09 and 1.2, respectively. Destruction in the NS4 solution is characterized by the appearance of flat fragments of different sizes; the main part of the composition is from the rupture of united small dimples, the other part is from individual facets of fragile origin. Deeply developed pits are observed, including from non-metallic inclusions, which are more concentrated in the zone close to the surface of the specimen, and are obviously a consequence of the action of the mechanism of local anodic dissolution.

Most of the failure surface of the specimen in the NS4-based model soil environment corresponds to a narrow shear failure, but at low energy.

Shear failure can characterize the formation of non-homogeneous areas of the surface as a result of failure under the action of a corrosive environment. On the fracture surface, the formation of a large number of brittle areas in the form of quasi-crack facets (up to 25 mm) and isolated local zones in the form of deep brittle damage to the surface was noted. This nature of destruction confirms the joint action of the mechanism of local anodic dissolution and the hydrogen mechanism in the model soil environment.

At the maximum protective potential of -1.050 V, stress-corrosion cracking of X70 steel in the NS4 solution occurs by a mixed mechanism, and in the soil environment based on NS4 – by the hydrogen mechanism, which correlates with the corresponding values of the coefficient of susceptibility to stress-corrosion cracking K_s in the model soil environment than in NS4 solution, 1.15 and 1.24, respectively. The mixed nature of the fracture in the solution is confirmed by the appearance of the fracture surface, which differs from the fracture surface at potentials of -0.750 V and -0.950 V. Under these conditions, along with the areas of rupture of small united pores, the proportion of brittle flat fragments up to 30 μm increased (facets of chipping, intergranular destruction). After specimen rupture in model soil environment, flat areas of a larger area (approximately 110 μm) were found in the fracture, which are significantly larger compared to fractures at potentials of -0.750 and -0.950 V. This indicates the predominant action of the hydrogen mechanism.

Considering the above, in a model soil environment based on NS4, one can expect more intensive hydrogenation at a lower cathodic polarization.

At a polarization potential range negatively than the maximum protective potential -1.200 V, stress-corrosion cracking in both environments occurs by the hydrogen embrittlement mechanism, but in the model soil environment based on NS4, the coefficient of susceptibility to stress-corrosion cracking is higher than in the solution, 1.54 and 1.4. The near-surface zone after tests in the NS4 solution consists mainly of brittle flat facets of approximately the same size (about 20 μm), which, as it approaches the middle, changes to a mixture of pitted fracture areas and part of small flat zones of brittle origin.

After tests in the soil environment, the surface of the fracture has long depressions, large pits, which are located between the areas of small-pit breaks, which indicates a local change of the surface under the influence of the environment and cathodic polarization, and is due to the penetration of hydrogen into the local metal zones, which is more intense compared to the solution.

5. CONCLUSIONS

The peculiarities of stress-corrosion cracking of X70 pipe steel under conditions of thin-layer corrosion in a soil environment with near neutral pH were investigated.

1. Corrosion potentials in the solution NS4 are more negative than in the model soil environment based on NS4, -0.737 mV and -0.704 V, respectively. The corrosion rates in both environments are similar, but in the model soil environment the corrosion rate is 5 % higher: 0.0536 in the NS4 solution and 0.0563 mm/year in the soil environment. The mechanism of anodic dissolution does not change, as confirmed by the slopes of the anodic curves, 0.063 V in the NS4 solution and 0.059 V in the model soil environment based on NS4.

2. It was established that there are three ranges of potentials in which the mechanism of stress-corrosion cracking of X70 steel changes in NS4 solution and in a model soil environment based on NS4. These ranges differ in solution and in the model soil environment. In the NS4 solution in the range of potentials, -1.001 V, stress-corrosion cracking proceeds by the mechanism of anodic dissolution, at potentials more negative than -1.085 V – by the mechanism of hydrogen embrittlement, in the range of potentials from -1.001 V to -1.085 V, stress-corrosion cracking proceeds by the mixed mechanism – anodic dissolution and hydrogen embrittlement. Accordingly, in the model soil environment the ranges are: more positive than -0.926 V, from -0.926 V to -1.050 V, and more negative than -1.050 V.

An expansion of the range of the mixed mechanism action for the soil environment based on NS4 to 0.124 V compared to the solution, 0.084 V, was noted.

3. At a minimum protective potential of -0.750 V and a polarization potential negatively the maximum protective potential of -1.200 V, the patterns of stress-corrosion cracking in the NS4 solution and in the model soil environment based on NS4 are similar, but in the model soil environment based on NS4, the susceptibility coefficient to stress-corrosion cracking K_s is higher in value.

4. Differences in the stress-corrosion cracking mechanism of X70 steel at potentials of -0.950 V

and -1.050 V in NS4 solution and in a model soil environment based on NS4 were established. At a potential of -0.950 V, stress-corrosion cracking of X70 steel in the NS4 solution proceeds by the mechanism of anodic dissolution, and in the model soil environment – by the mixed mechanism. At the maximum protective potential of -1.050 V, stress-corrosion cracking of X70 steel in the NS4 solution occurs by a mixed mechanism, and in the NS4-based soil environment by the hydrogen embrittlement mechanism. The obtained regularities are confirmed by the values of the coefficients of susceptibility to stress-corrosion cracking K_s and the results of the fractographic analysis of fracture surfaces.

Acknowledgements

This work was carried out in E.O. Paton Electric Welding Institute of the National Academy of Sciences of Ukraine with financial support by the National Academy of Sciences of Ukraine in 2022-2024 (State registration number 0122U001188).

6. REFERENCES

[1] S. Cole, D. J. C. S. Marney (2012) The science of pipe corrosion: A review of the literature on the corrosion of ferrous metals in soils, *Corrosion science*, *56*, 5-16. https://doi.org/10.1016/j.corsci.2011.12.001

[2] K. Yin, H. Liu, Y. F. Cheng (2018) Microbiologically influenced corrosion of X52 pipeline steel in thin layers of solution containing sulfate-reducing bacteria trapped under disbonded coating, *Corrosion Science*, 145, 271-282. https://doi.org/10.1016/j.corsci.2018.01.029

[3] M. Wasim, S. Shoaib, N. Mubarak, M. Inamuddin, A. M. Asiri (2018) Factors influencing corrosion of metal pipes in soils, *Environmental Chemistry Letters*, *16*, 861-879. https://doi.org/10.1007/s10311-018-0731-x

[4] S. Suganya, R. Jeyalakshmi (2019) Corrosion of mild steel buried underground for 3 years in different soils of varying textures, *Journal of Materials Engineering and Performance*, *28*, 863-875. https://doi.org/10.1007/s11665-019-3855-7

[5] H. M. Ezuber, A. Alshater, S. Z. Hossain, A. El-Basir (2021) Impact of soil characteristics and moisture content on the corrosion of underground steel pipelines, *Arabian J. for Science and Engineering*, 46, 6177-6188. https://doi.org/10.1007/s13369-020-04887-8

[6] L. Zhang, X. G. Li, C. W. Du (2009) Effect of environmental factors on electrochemical behavior of X70 pipeline steel in simulated soil solution, *Journal of Iron and Steel Research International*, 16(6), 52-57. https://doi.org/10.1016/S1006-706X(10)60027-1

[7] J. Jiang, J. Wang, Y. H. Lu, J. Z. Hu (2009) Effect of length of gas/liquid/solid three-phase boundary zone on cathodic and corrosion behavior of metals, *Electrochimica Acta*, *54*(5), 1426-1435. https://doi.org/10.1016/j.electacta.2008.09.017

[8] H. Liu, Y. Dai, Y. F. Cheng (2020) Corrosion of underground pipelines in clay soil with varied soil layer thicknesses and aerations, *Arabian Journal of Chemistry*, *13*(2), 3601-3614. https://doi.org/10.1016/j.arabjc.2019.11.006

[9] S. Wang, C. Du, X. Li, Z. Liu, M. Zhu, D. Zhang (2015) Field corrosion characterization of soil corrosion of X70 pipeline steel in a red clay soil, *Progress in Natural science: Materials international*, 25(3), 242-250. https://doi.org/10.1016/j.pnsc.2015.06.006

[10] Y. Song, G. Jiang, Y. Chen, P. Zhao, Y. Tian (2017) Effects of chloride ions on corrosion of ductile iron and carbon steel in soil environments, *Scientific reports*, *7*(1), 6865. https://doi.org/10.1038/s41598-017-07245-1

[11] X. Bai, B. He, P. Han, R. Xie, F. Sun, Z. Chen, X. Liu (2022) Corrosion behavior and mechanism of X80 steel in silty soil under the combined effect of salt and temperature, *RSC advances*, 12(1), 129-147.https://doi.org/10.1039/D1RA08249C

[12] Z. Y. Liu, Q. Li, Z. Y. Cui, W. Wu, Z. Li, C. W. Du, X. G. Li (2017) Field experiment of stress corrosion cracking behavior of high strength pipeline steels in typical soil environments, *Construction and Building Materials*, 148, 131-139. https://doi.org/10.1016/j.conbuildmat.2017.05.058

[13] A. Q. Fu, X. Tang, Y. F. Cheng (2009) Characterization of corrosion of X70 pipeline steel in thin electrolyte layer under disbonded coating by scanning Kelvin probe, *Corrosion Science*, 51 (1), 186-190. https://doi.org/10.1016/j.corsci.2008.10.018

[14] M. Yan, J. Wang, E. H. HAN, C. Sun, W. Ke (2014) Characteristics and evolution of thin layer electrolyte on pipeline steel under cathodic protection shielding disbonded coating, *Acta Metallurgica Sinica*, 50(9), 1137-1145. https://doi.org/10.11900/0412.1961.2014.00156

[15] K. Gong, M. Wu, F. Xie, G. Liu, D. Sun (2020) Effect of dry/wet ratio and pH on the stress corrosion cracking behavior of rusted X100 steel in an alternating dry/wet environment, *Construction and Building Materials*, 260, 120478. https://doi.org/10.1016/j.conbuildmat.2020.120478

[16] L. I. U. Zhiyong, L. I. Xiaogang, Y. Zhang, D. U. Cuiwei, Z. H. A. I. Guoli (2009) Relationship between electrochemical characteristics and SCC of X70 pipeline steel in an acidic soil simulated solution, *Acta Metallurgica Sinica (English Letters)*, 22(1), 58-64. https://doi.org/10.1016/S1006-7191(08)60071-X

[17] R. Hendi, H. Saifi, K. Belmokre, M. Ouadah, B. Smili, B Talhi (2018) Effect of black clay soil moisture on the electrochemical behavior of API X70 pipeline steel, *Materials Research Express*, 5 (3), 036523. https://doi.org/10.1088/2053-1591/aab40e

[18] ISO 3183:2019 Petroleum and natural gas industries — Steel pipe for pipeline transportation systems

[19] Antunes de Sena R, Napoleão Bastos I, Mendes Plat G. (2012) Theoretical and Experimental Aspects of the Corrosivity of Simulated Soil Solutions.*International Scholarly Research Notices,* 6, 103715. https://downloads.hindawi.com/archive/2012/103715.pdf

[20] L. I. Nyrkova, A. V. Klymenko, S. O. Osadchuk, S. Y. Kovalenko (2024) Comparative investigation of electrolytic hydrogenation of pipe assortment steel under cathodic polarization, *International Journal of Hydrogen Energy*, 49, 1075-1087. https://doi.org/10.1016/j.ijhydene.2023.06.316.

[21] L. I. Nyrkova, A. V. Klymenko, L. V. Goncharenko, S. O. Osadchuk, S. Y. Kovalenko, Y. O. Kharchenko, V. V. Lavrenyuk (2023) Influence of electrolytic hydrogenation on stress-corrosion cracking of X70 steel and pipes of long-term exploited main gas pipeline, *Journal of hydrocarbon power engineering*, 10 (1), 15-24. https://doi.org/10.31471/2311-1399-2023-1(19)-15-24

[22] L. Nyrkova (2020) Stress-corrosion cracking of pipe steel under complex influence of factors, *Engineering Failure Analysis*, 116, 104757. https://doi.org/10.1016/j.engfailanal.2020.104757.

[23] L. Nyrkova, S. Osadchuk (2023) Stress-corrosion cracking of the steels of main gas pipeline: assessment and prevention. Kyiv, Naukova Dumka. p.216. [in Ukrainian]. https://doi.org/10.15407/978-966-00-1845-7

[24] National Standard of Ukraine4219-2003 STEEL PIPE MAINS. General requirements for corrosion protection. Kyiv, 2003. p.86.

IZVOD

UTICAJ TANKOSLOJNIH USLOVA NA NAPREZNO-KOROZIJSKO PUCANJE ČELIKA X70 BLIZU NEUTRALNOG pH PRI KATODNOJ POLARIZACIJI

Prioritetni zadatak savremenih podzemnih magistralnih cevovoda je da obezbedi pouzdanost njegovog rada, što u velikoj meri zavisi od razumevanja procesa koji se dešavaju na površini cevi u zemlji u uslovima katodne zaštite. Svrha ovog rada je da se prouče karakteristike pucanja od naponske korozije (SCC) čelika X70 u uslovima tankoslojne korozije u okruženju blizu neutralnog pH. Korišćeni su potenciometrija, voltametrija, masometrija, elektrolitička hidrogenacija spore brzine deformacije, skenirajuća elektronska mikroskopija. Eksperimentalno su utvrđene razlike u SCC mehanizmu čelika X70 na potencijalima od -0,950 V i -1,050 V u ispitivanim sredinama. Na -0,950 V, SCC čelika X70 u NS4 se odvija mehanizmom anodnog rastvaranja, a u okruženju modelnog tla - mešovitim mehanizmom; na -1,050 V, SCC u rastvoru NS4 nastaje mešovitim mehanizmom, a u zemljištu zasnovanom na NS4 – mehanizmom vodoničnog krtenja. Dobijene pravilnosti su posledica značajnijeg krtenja pri površinskog sloja uzoraka u okruženju modelnog tla u tankim slojevima pod katodnom polarizacijom, što dovodi do promene mehanizma SCC od plastično krhkog do potpuno krhkog.

Ključne reči: *čelik za cevi, ispitivanja sporog deformisanja, potenciometrija, voltametrija, naponsko-koroziono pucanje, tankoslojna korozija, hidrogenacija*

Naučni rad
Rad primljen: 11.01.2025
Rad prihvaćen: 23.01.2025.

Lyudmila Nyrkova, https://orcid.org/0000-0003-3917-9063
Larysa Goncharenko, https://orcid.org/0000-0001-8371-2078
Svetlana Osadchuk, https://orcid.org/0009-0009-4968-4777
Oleg Bratochkin, https://orcid.org/0009-0001-5710-3460